2004

Are Microbubbles Necessary for the Breakdown of Liquid Water Subjected to a Submicrosecond Pulse?

R. P. Joshi
Old Dominion University

J. Qian
Old Dominion University

G. Zhao
Old Dominion University

J. Kolb
Old Dominion University

K. H. Schoenbach
Old Dominion University

See next page for additional authors

Original Publication Citation

Joshi, R. P., Qian, J., Zhao, G., Kolb, J., Schoenbach, K. H., Schamiloglu, E., & Gaudet, J. (2004). Are microbubbles necessary for the breakdown of liquid water subjected to a submicrosecond pulse? *Journal of Applied Physics, 96*(9), 5129-5139. doi:10.1063/1.1792391

Are microbubbles necessary for the breakdown of liquid water subjected to a submicrosecond pulse?

R. P. Joshi,[a] J. Qian, G. Zhao, J. Kolb, and K. H. Schoenbach
Department of Electrical and Computer Engineering Old Dominion University, Norfolk, Virginia 23529-0246

E. Schamiloglu and J. Gaudet
Department of Electrical and Computer Engineering, University of New Mexico, Albuquerque, New Mexico 87131

(Received 7 June 2004; accepted 16 July 2004)

Electrical breakdown in homogeneous liquid water for an ~100 ns voltage pulse is analyzed. It is shown that electron-impact ionization is not likely to be important and could only be operative for low-density situations or possibly under optical excitation. Simulation results also indicate that field ionization of liquid water can lead to a liquid breakdown provided the ionization energies were very low in the order of 2.3 eV. Under such conditions, an electric-field collapse at the anode and plasma propagation toward the cathode, with minimal physical charge transport, is predicted. However, the low, unphysical ionization energies necessary for matching the observed current and experimental breakdown delays of ~70 ns precludes this mechanism. Also, an ionization within the liquid cannot explain the polarity dependence nor the stochastic-dendritic optical emission structures seen experimentally. It is argued here that electron-impact ionization within randomly located microbubbles is most likely to be responsible for the collective liquid breakdown behaviors. © *2004 American Institute of Physics*. [DOI: 10.1063/1.1792391]

I. INTRODUCTION

There is a considerable interest in the study of electrical breakdown in water (and other liquids) for a variety of reasons.[1] Practical applications of dielectric liquids include switching elements for pulsed power systems,[2] use in energy storage, as water-filled gaps for the design of acoustic equipment,[3,4] the insulation of high-voltage devices,[5] and as the medium in spark erosion machines.[6] Generally, for high-voltage-pulsed power systems, solids or gases at high pressure have been used as the dielectric material. However, the use of polar liquids seems to have advantages for both energy storage and switch media, particularly for the nanosecond pulse generators. Polar liquids not only have a high dielectric constant but have also a higher breakdown strength than compressed gases.[7] Water, for example, has been used and found to hold off electrical fields beyond 1 MV/cm for durations up to hundreds of nanosecond.[8,9] In comparison to solids, their ability to circulate leads to a better thermal management and easier removal of debris after breakdown. Liquid dielectrics are also better suited for applications involving complex geometries.

The electrical behavior of dielectric liquids (especially water) subjected to high electric fields has been intensively studied,[11–19] especially for voltage durations of microseconds or longer. Despite a large body of experimental observations, there is still no comprehensive understanding of the inherent breakdown physics. Part of the problem is that liquids lack the long-range order and periodicity that are inherent in solids. Also, in contrast to gases, the molecular density is much higher, which significantly enhances the collective clustering effects and formation of trimers, tetramers, and pentamers.[20,21] Water breakdown presents a complex and dynamical, many-body problem. Another complication is that conduction is strongly influenced by both the liquid-electrode interface and bulk properties that include a variety of electric-field and temperature-dependent processes.[22–24] For relatively long-voltage pulse durations of microseconds or higher, two competing theories of liquid breakdown in water have emerged: (i) A bubble-initiated breakdown process and (ii) an electronic impact-ionization process. For such long-voltage pulses, it is postulated that liquid electrical breakdown proceeds through the creation and propagation of streamers over regions of low density.[16,25–28] The propagation of streamers during water breakdown is explained on the basis of liquid water evaporation at the tip of the streamer due to substantial local heating.[23]

The proposed electron-initiated mechanism does not appear to be very plausible for several reasons: (i) Firstly, electron avalanche processes in liquids are nearly negligible.[10] As our own calculations in this contribution will demonstrate, relatively high scattering cross sections coupled with the largely isotropic elastic scattering excludes the possibility for the electrons in water to acquire significant kinetic energy for impact ionization. The electrons are most likely to undergo a large number of random scattering events (i.e., exhibit a very short mean free path), and quickly attach to neutral molecules to form "electron bubble,"[29,30] or recombine with positive ions. (ii) Secondly, free electrons are generally absent in water because an enormous increase in entropy is required to convert an electron into a negative ion by attachment. This dearth of free electrons can alternatively be viewed as arising from the large "band gap" of water, which

[a]Electronic mail: rjoshi@odu.edu

is ~8.5 eV,[31] and the high barrier height between the metal-liquid interface. Furthermore, recent experimental data clearly shows that free electrons are quickly solvated within ~1 ps time scales.[32] Hence, the probability for a free-electron population is likely to be negligible. (iii) Finally, the observed dependence of breakdown on hydrostatic pressure and voltage pulse duration point toward the predominance of the vapor bubble formation process. For example, a high hydrostatic pressure inhibits bubble formation resulting in an observed increase of the hold-off strength.[33] Similarly, since longer pulses allow more time for bubble nucleation, they lead to decreases in the required breakdown field.

A scenario of internal heating with bubble formation can only be possible if the duration of the applied voltage is sufficiently long, i.e., at least in the 10–100 μs range or larger. In recent experiments within our research group and elsewhere, the breakdown of water-filled switches has been observed with short 200 ns voltage pulses.[2,9] This time duration is too small for any significant heating. Temperature increases of less than 6 K are predicted[34] for these situations. Moreover, a simple application of the electrostatic image method demonstrates that charged particles immersed in the high dielectric water medium cannot penetrate to any naturally occurring microbubbles, due to the inherent electrostatic Coulomb repulsion.[35] Hence, a separate mechanism, differing from the traditional viewpoint, has to be considered for the initiation of breakdown in liquids by a short, submicrosecond electrical pulse. A possibility is the natural existence of a random distribution of microbubbles within the liquid due to dissolved gases, even in the absence of any internal heating.

A second important issue in the liquid breakdown concerns the distinct polarity effects.[1,36–39] For example, in the wire-plane geometry that has been extensively studied, two types of behaviors are exhibited depending on whether the wire electrode is the anode or the cathode. In case of a wire anode (positive polarity), the breakdown is accompanied by bushy filamentary streamers and optical emission. In general, the streamer propagation velocity is voltage dependent and displays several modes.[40] The negative biasing of the wire electrode, on the other hand, leads to a higher voltage requirement for breakdown,[41] and streamers take longer to form. The geometric form of the streamers is also different. Such a polarity dependence is not well understood, and a physical basis remains elusive. Based on gas discharge physics, one might expect the liquid water breakdown to be initiated at the cathode due to possible contributions of electronic injection. The experimental data, however, suggests otherwise, and instead indicates that other mechanisms must be relevant to the breakdown process.

Here, we attempt to seek, probe, and quantitatively investigate the possibility of electrical breakdown and the polarity effects on the basis of the on-going physical processes in a homogeneous liquid medium. It will be shown that the breakdown in a homogeneous medium (e.g., without any air bubbles) is difficult and would require much higher applied voltages than the experimentally observed. In our study, we include details of the field-assisted charge transport at the liquid-metal interface and asymmetries at the cathode and anode based on the differences in the energy levels of positive and negative ions (for example, OH^- and H_3O^+). For example, positive ions favor electronic transitions by forming potential wells for electrons, whereas negative ions present repulsive barriers. Hence, cathodes, for example, can be expected to have relatively larger conduction currents as compared to anodes. Consequently, cathode neighborhoods would not facilitate as large a displacement current and associated buildup of electric fields. Conduction across the anode is shown here to be strongly field controlled with a sharp switchlike characteristic in the conductance.

On the basis of Monte Carlo calculations, it is also shown that free-electron transport and possible impact ionization by electrons would be virtually absent for short-pulse conditions. The electron-initiated processes can only become possible at low water density, as might arise, for example, through a heat-generated bubble formation or under nonthermal, nonequilibrium conditions of optical excitation.

We also investigate the possible role of field ionization (the Zener-tunneling process) in water as a mechanism for charge creation. Field ionization (or field assisted, intermolecular electron transfer) can be expected to initiate within the regions of the highest electric field. In the absence of internal inhomogeneities, the likely location of high electric stresses would be at the electrodes due to the space-charge and geometric field-enhancement effects. The high interface fields can be expected to be further enhanced by field-dependent decreases in dielectric constant due to dipole orientational effects.[42] Our simulations demonstrate that for the field ionization to be responsible for the water breakdown in keeping with the experimental observations, the ionization energy needs to be in the order of 2.3 eV. Based on this process, an electric-field collapse at the anode with a fast propagation toward the cathode side is predicted. However, if the ionization energies are actually much larger (as in the case of an isolated water molecule), then different processes such as internal microbubble distributions, Grotthuss type,[43] field-modulated mobility mechanisms, or intermolecular electron transfers associated with local potential fluctuation might be at work. The exact ionization energy parameter is difficult to ascertain because it is determined by the collective many-body effects and the local molecular structure, and so, could quite possibly be a random variable about a fixed mean value.

II. MONTE CARLO ANALYSIS TO ASSESS POSSIBLE ELECTRON-INITIATED IONIZATION IN LIQUID WATER

In theory, the impact ionization by energetic electrons emitted from the cathode could be considered a possible route for liquid breakdown. While this likelihood has been suggested in the past, we are not aware of any detailed analysis or evaluation of this process. This has partly been due to the unavailability of various scattering cross sections. Though reports of Monte Carlo simulations for water vapor have existed,[44] cross sections for the high-density liquid water became known only very recently.[45]

Here, we carry out three-dimensional, time-dependent Monte Carlo analyses of cathode initiated, electron transport

in liquid water. The details such as the electron energy distribution, the possibility of secondary electron generation, drift velocities, and spatial distribution of injected electron swarms are evaluated. Electrons in liquid water undergo an energy-dependent scattering that can be either elastic, inelastic ionization, or inelastic excitation.[45] The latter includes transitions toward the Rydberg or degenerate states, attachment leading to negative-ion generation, vibrational and rotational excitations, and excitation of the OH^*, H^*, and O^* radicals. In our analysis, the energy-dependent cross sections $S(E)$ were parameterized based on a recent data report.[45] The following mathematical expressions with the cross section S in units of per square centimeter and the energy E in units of electron volt were obtained. For elastic scattering

$$\log_{10}(S) = 0.06769[\log_{10}(E)]^3 + 0.4833[\log_{10}(E)]^2 - 1.848[\log_{10}(E)] - 13.288. \quad (1)$$

For ionization, the following piecewise curve fit resulted in:

$$S = \{13.86[\log_{10}(E)]^5 - 106.6[\log_{10}(E)]^4 + 319.4[\log_{10}(E)]^3 - 465.5[\log_{10}(E)]^2\} \times 10^{-16} + \{333.6[\log_{10}(E)] - 95.11\} \times 10^{-16}, \quad (2a)$$

for $13.5\ \text{eV} < E < 120\ \text{eV}$ and

$$S = \left\{ \begin{array}{c} 0.6391[\log_{10}(E)]^6 - 12.20[\log_{10}(E)]^5 + 95.25[\log_{10}(E)]^4 \\ - 388.4[\log_{10}(E)]^3 + 871.1[\log_{10}(E)]^2 - 1019[\log_{10}(E)] + 488.5 \end{array} \right\} \times 10^{-16} \quad (2b)$$

for $120\ \text{eV} < E < 10^4\ \text{eV}$.

There are a number of collective excitation processes that can occur (for example, Ref. 45). We have parameterized all of them, but for brevity, we have provided expressions for only the most dominant ones. The cross sections for electronic scattering toward the degenerate states $\overline{A}_1B_1$ were obtained as follows:

$$\log_{10}(S) = -237.4[\log_{10}(E)]^4 + 1122[\log_{10}(E)]^3 - 1991[\log_{10}(E)]^2 + 1574[\log_{10}(E)] - 486.0 \quad (3a)$$

for $10\ \text{eV} < E < 20\ \text{eV}$,

$$\log_{10}(S) = -0.1323[\log_{10}(E)]^4 + 1.471[\log_{10}(E)]^3 - 6.048[\log_{10}(E)]^2 + 10.21[\log_{10}(E)] - 22.94 \quad (3b)$$

for $20\ \text{eV} < E < 500\ \text{eV}$.

The cross sections for electronic scattering toward the degenerate states $B_1\overline{A}_1$ were obtained as follows:

$$\log_{10}(S) = 5187[\log_{10}(E)]^5 - 31057[\log_{10}(E)]^4 + 74387[\log_{10}(E)]^3 - 89107[\log_{10}(E)]^2 + 53400[\log_{10}(E)] - 12830. \quad (4a)$$

for $10\ \text{eV} < E < 20\ \text{eV}$.

$$\log_{10}(S) = -0.6091[\log_{10}(E)]^4 + 5.453[\log_{10}(E)]^3 - 18.47[\log_{10}(E)]^2 + 27.42[\log_{10}(E)] - 31.79 \quad (4b)$$

for $20\ \text{eV} < E < 500\ \text{eV}$.

From the electronic transitions to the diffuse band, the parameterized cross sections were obtained as follows:

$$\log_{10}(S) = \{1.558[\log_{10}(E)]^5 - 10.14[\log_{10}(E)]^4 + 26.40[\log_{10}(E)]^3 - 34.35[\log_{10}(E)]^2\} \times 10^4 + \{22.34[\log_{10}(E)] - 5.813\} \times 10^4, \quad (5a)$$

for $14\ \text{eV} < E < 25\ \text{eV}$,

$$\log_{10}(S) = -0.6056[\log_{10}(E)]^4 + 5.881[\log_{10}(E)]^3 - 21.46[\log_{10}(E)]^2 + 34.29[\log_{10}(E)] - 36.59, \quad (5b)$$

for $25\ \text{eV} < E < 500\ \text{eV}$.

The cross sections of electron scattering into the Rydberg states were obtained as follows:

$$\log_{10}(S) = 0.2386[\log_{10}(E)]^5 - 3.128[\log_{10}(E)]^4 + 16.11[\log_{10}(E)]^3 - 40.89[\log_{10}(E)]^2 + 50.81[\log_{10}(E)] - 41.62, \quad (6a)$$

for $20\ \text{eV} < E < 2000\ \text{eV}$, and

$$\log_{10}(S) = -1.021[\log_{10}(E)] - 14.64, \quad (6b)$$

for $E > 2000\ \text{eV}$.

The cross sections for dissociative excitation were curve fit according to the following:

$$\log_{10}(S) = \{1.062[\log_{10}(E)]^5 - 7.428[\log_{10}(E)]^4 + 20.75[\log_{10}(E)]^3 - 28.96[\log_{10}(E)]^2\} \times 10^3 + \{20.19[\log_{10}(E)] - 5.643\} \times 10^3, \quad (7a)$$

for $14\ \text{eV} < E < 35\ \text{eV}$,

$$\log_{10}(S) = -1.004[\log_{10}(E)] - 15.60, \quad (7b)$$

for $E > 35\ \text{eV}$.

Finally, for the dissociative attachment leading to the formation of H^-, which is the strongest of all the electron

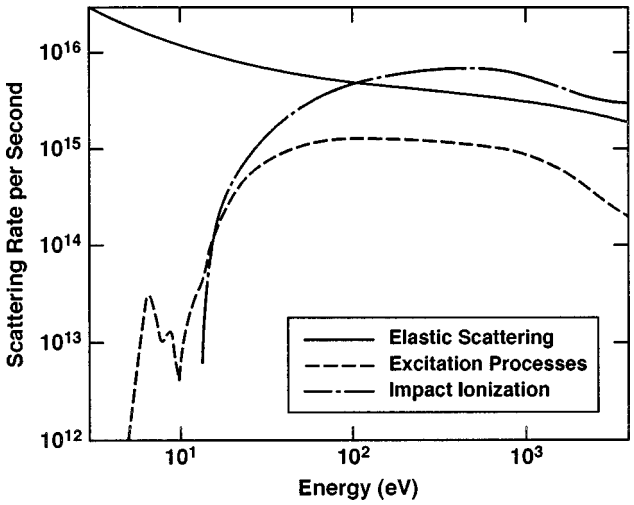

FIG. 1. Energy-dependent elastic and inelastic scattering rates used for the electron Monte Carlo scattering.

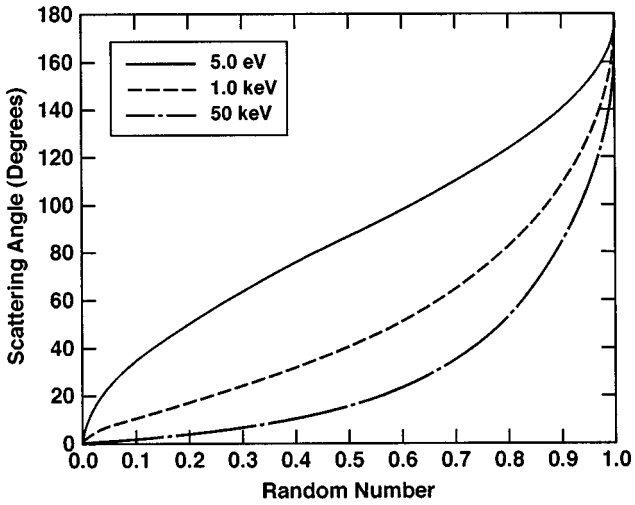

FIG. 2. Angular distribution with random number for elastic scattering for three different electron energies.

attachment processes, the parameterized equation for the 4–11 eV range, with zero values elsewhere was obtained as follows:

$$S = (5.083E^4 - 90.16E^3 + 599.7E^2 - 1771E + 1958) \times 10^{-19}, \tag{8a}$$

for $4\ \text{eV} < E < 6\ \text{eV}$,

$$S = (1.569E^4 - 41.13E^3 + 402.6E^2 - 1744E + 2824) \times 10^{-17}, \tag{8b}$$

for $6\ \text{eV} < E < 7\ \text{eV}$,

$$S = (0.5958E^4 - 20.97E^3 + 275.4E^2 - 1600E + 3473) \times 10^{-18}, \tag{8c}$$

for $7\ \text{eV} < E < 9\ \text{eV}$,

$$S = (-4.032E^3 + 148.4E^2 - 1806E + 7275) \times 10^{-20}, \tag{8d}$$

for $9\ \text{eV} < E < 11\ \text{eV}$.

The energy-dependent scattering rates from the cross sections for elastic scattering, ionization, and all the excitation processes obtained from the previous polynomial fitting are shown in Fig. 1. At low energies, elastic scattering dominates, and can thus be expected to lead to low mobilities and electron energies. This is particularly true under the conditions of isotropic angular scattering.

The Monte Carla scheme is a stochastic, kinetic approach that involves the space-time dynamical evolution of a swarm of simulation particles. The particles are taken to obey Newtonian mechanics, and their movements consist of a series of free lights, peppered by random scattering events.[46] Based on the self-scattering (or the null scattering) technique, the stochastic free-flight time t_{FF} (or mean-time-to-collision) is obtained from the maximum scattering rate $R_{\max}$ as follows: $t_{FF} = -[\ln(r)]/R_{\max}$, where r is a random number and "ln" stands for the natural logarithm. The $R_{\max}$ value is obtained by taking the maximum of the various energy-dependent scattering rates $R_i(E)$ with all the elastic and inelastic processes taken into account. In general, the scattering rate $R(E)$ is related to the corresponding cross section $S(E)$ for that process obtained as follows: $R(E) = S(E)Nv(E)$, where N is the density of water molecules and $v(E)$ is the energy-dependent electron velocity. This scattering rate can also be used to crudely estimate the electron mobility μ for a thermal distribution of energies. In the collision-dominated regime, $\mu = q\langle\tau\rangle/m$, where $\langle\tau\rangle$ is the average collision time and m is the electron effective mass. Since roughly $\langle\tau\rangle \sim 1/\langle R\rangle$, the electron mobility works out about $6 \times 10^{-6}\ \text{m}^2/\text{V/s}$ for a thermalized energy distribution from the values of Fig. 1.

Monte Carlo simulations were carried out by injecting a swarm of 6000 particles from the cathode at a given electric field. The electric field was not updated (as done in usual "particle-in-cell" codes [47]) on the assumption of a low electronic charge density. The initial energies were assigned based on a thermalized Boltzmann distribution. A time step of 0.01 fs was used for the highest water density (i.e., 1 gm/cc) because of the high elastic scattering rate shown in Fig. 1. The angular distribution was taken to be isotropic for the inelastic processes. For elastic scattering, a Rutherford-Moliere [45] differential cross section $S(\theta)$ of the form

$$S(\theta) = K_1/[K_2 - \cos(\theta)], \tag{9}$$

was used, with K_1 and K_2 being the angle independent constants based on the energy, atomic number, and screening parameter.[45] From Eq. (9), the angle selection for the final state after elastic scattering can be ascertained from the distribution $S(\theta)$, by invoking a random number "r" and by using the following relation:

$$r = \left[\int_0^{\theta} S(\theta)\sin(\theta)d\theta\right] \Big/ \left[\int_0^{\pi} S(\theta)\sin(\theta)d\theta\right]. \tag{10}$$

Carrying out the integration leads to a closed form expression for the angle θ in terms of the random number "r." Figure 2 shows the angular distribution as a function of the random number for the three electron energies. As evident

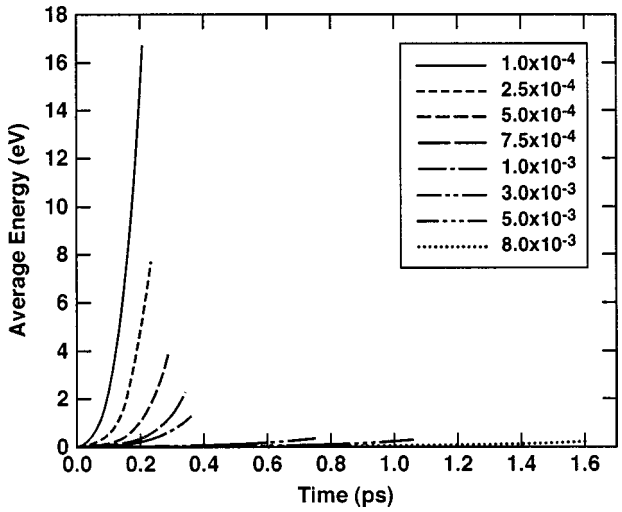

FIG. 3. Time-dependent Monte Carlo results showing the swarm kinetic energies at a 10^8 V/m field for various density factors F.

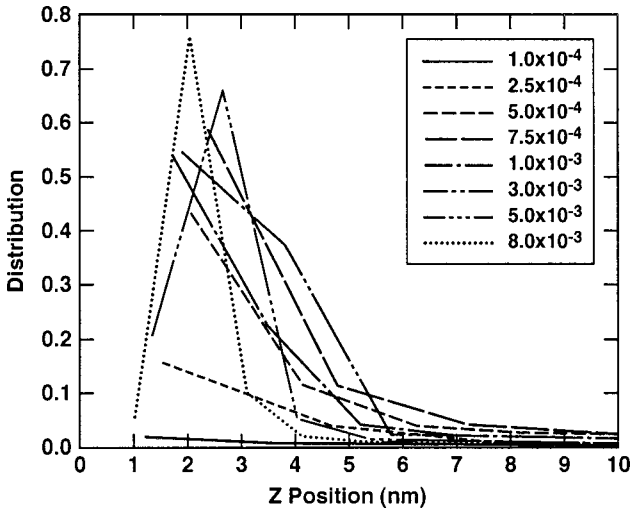

FIG. 4. Spatial distribution of the electron swarm from the cathode (at $z=0$) after 1.6 ps.

from the curves, the scattering is almost isotropic for small energies and shifts toward an anisotropic, small forward angle behavior only at very large energies. This essentially implies that the electrons injected from the cathode are likely to be heavily scattered in a random fashion and that they would be unable to pickup much energy. Their mobility would therefore remain close to the 6×10^{-6} $m^2/V/s$ value.

Clearly, the scattering rate depends on the liquid density N. The most favorable condition for energy gain, and arguably, a pathway to possible impact ionization occurs at low densities. This situation can occur for long-voltage pulses that can cause internal heating and bubble formation or under optical excitation. In order to ascertain the density dependence for possible impact ionization, we carried out Monte Carlo runs for different water density values (hence, different scattering rates) by releasing 6000 electrons from the cathode and following their trajectories for relatively short times. The distributions of the swarm in position and energy space, as well as the production of the secondary electrons due to ionization were monitored. Figure 3 shows the time-dependent mean swarm energy at a field of 10^8 V/m and various fractional density factors F (here $F=1$ indicates the normal water density). As the density is decreased, the scattering rates scale down to lower values, thereby increasing the velocity and energy of the particles. A snapshot of the spatial electron swarm distribution from the cathode (at $z=0$) after 1.6×10^{-12} s is shown in Fig. 4. Most particles are seen to still lie near the cathode. For the higher F values (corresponding to the highest scattering and smallest mobility), the distribution is bunched more tightly and shows a peak toward the low z values.

The number of impact ionization events for the 10^8 V/m field are given in Fig. 5. At the highest density factor of 0.006, substantial numbers of secondary-charge carriers are predicted within a relatively short time. However, increasing the density factor to about 0.01 (not shown) resulted in almost no ionization event, and a very low drift velocity. In our simulations, higher electric fields were also used, and the corresponding upper bound on F required for initiating ionization events decreased. Figure 6 shows a plot of the electric field versus the maximum allowable density factor for ionization. For the peak breakdown fields of about 4×10^9 V/m for the water observed experimentally,[2,9] our results indicate that normal water densities would be too high to facilitate the ionizing avalanche necessary for triggering the breakdown. This clearly demonstrates that electron injection at the cathode cannot play a dominant part in the breakdown for the short-pulse conditions, and is only likely to produce slow moving negative ions (through trapping or attachment), or quasi-localized electron bubbles.

III. ENERGY-BAND MODEL FOR LIQUID WATER

We next examine the breakdown phenomena and related polarity effects based on an energy-band model for homogeneous liquid water. Such energy-band approaches have been used in the past.[31,48] Figure 7(a) shows a simple schematic of the bands under zero-field, equilibrium conditions. Based on published data,[31] water was taken to have a band gap of

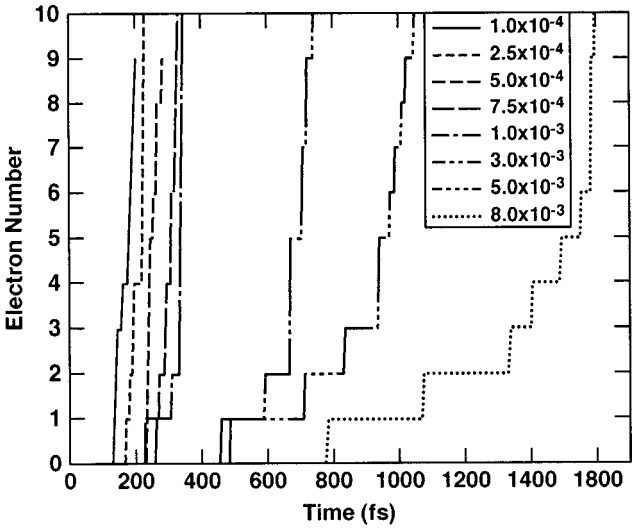

FIG. 5. Time evolution of the number of ionization events for a 10^8 V/m field and various density factors.

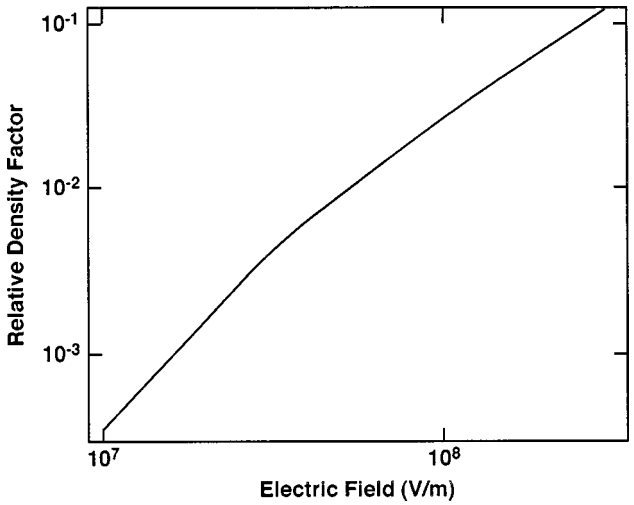

FIG. 6. Monte Carlo calculation of the water density factor vs the maximum electric field required for ionizing multiplication.

8.5 eV and an electron affinity of ~0.8 eV. For common electrode materials (e.g., stainless steel, brass etc.), the metal work function is near 4.5 eV. Space-charge effects and a built-in electric filed (with opposing directionality) will occur at both electrodes under these conditions. Obviously, for a small work function, the band bending and space-charge polarity at the metal interfaces would be reversed. At high bias, the band would change as sketched in Fig. 7(b), and a unidirectional field would prevail.

Breakdown usually implies a sudden rise in the carrier density (though a dramatic increase in mobility would have a similar effect), and the following sources for charge creation

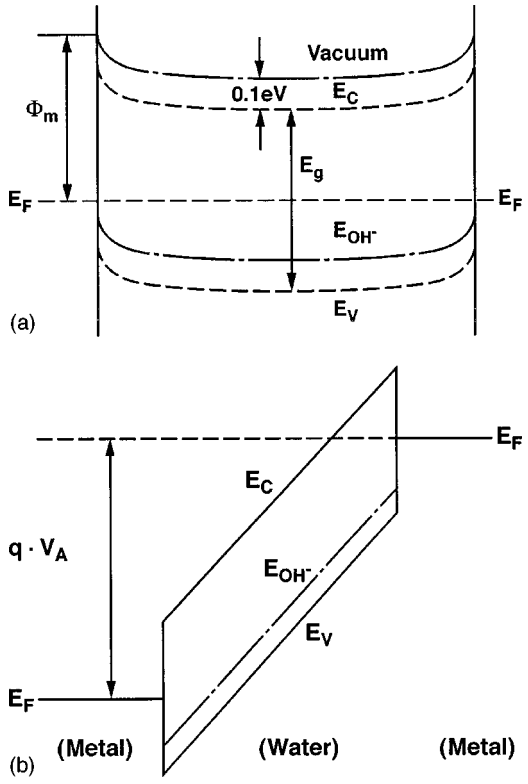

FIG. 7. Energy-band representation for liquid water. (a) zero bias, equilibrium condition and (b) with external bias.

and/or injection exist, as sketched in Fig. 8. (i) Electronic injection from the cathode [processes "4" or "5" of Fig. 8(a)] can lead to the formation of negative ions due to electron capturing trapping (because impact ionization cannot occur as already shown). There could also be an annihilation of positive ions [process "1" of Fig. 8(a)]. In theory, electronic injection can occur either via the tunneling of cold electrons [process "5" of Fig. 8(a)], or thermionic emission, or injection of hot electrons due to an Auger effect [processes "1–4" of Fig. 8(a)]. Of these, the thermionic emission can be neglected due to the near-thermal conditions for the present short-pulse scenario. Cold electron tunneling is also not likely due to the relatively large energy barrier to the conduction band. The Auger processes 1–4 are also likely to be weak because this process requires that the electron transition "2" be quite strong to provide the energy boost for process "3." However, the electron populations close to the Fermi level will be much smaller than those at much lower energies. Hence, transition "2" from a level close to the Fermi level is not as likely as the localized shuffling of metallic electrons in the vicinity of level "1". The cathode can be expected to primarily supply current due to process "1", resulting in direct electronic transitions from the metal to the positive ionic sites. Here, we have assumed that only process "1" is of significance. This will produce a conduction current that limits the displacement component and prevents large increases in electric fields near the cathode.

Electronic charge-transfer processes occurring near the anode include: (i) Electron transfer via tunneling at the anode from negative ions, as shown in Fig. 8(b). In general, numerous negative ions such as OH^-, $C1^-$, and I^- can exist near the anode. For simplicity, only the OH^- ion is considered here, with an energy separation of about 0.7 eV from the valence band.[31] This assumes nearly pure water, and as such, represents an idealized limiting condition. As evident from Fig. 8(b), the OH^- ions in a very close proximity to the anode would be unable to transfer electrons due to the near complete state filling of the metallic band. A significant field dependence to the charge transfer from the OH^- ions is to be expected due to the band bending. (ii) Field ionization [49] due to the tunneling of electrons from neutral water molecules as sketched in Fig. 8(c). As seen in Fig. 8(c), the effective energy barrier to the electron transfer process can be fairly small in the order of ~2–3 eV. This field ionization rate R_I is strongly field dependent and roughly given as follows.[39,50]

$$R_I = [(qEa)/h]\exp[-(ma\pi^2\Delta^2)/(qEh^2)], \tag{11}$$

where h is the Planck's constant, a is the molecular separation (~0.31 nm for water at normal densities), q is the electronic charge magnitude, and Δ is the ionization energy barrier for water. Generally, the ionization potential for an isolated water molecule is quite large.[51] However, as shown recently, the clustering of water molecules, combined with the presence of an external field, effectively leads to a significant energy lowering.[51] Here, we treat the energy barrier as a fitting parameter and seek to obtain the numerical value that would yield a good agreement with the experimental results. Based on Fig. 8(c), field ionization can lead to a continuous transfer of electrons in a sequential hopping man-

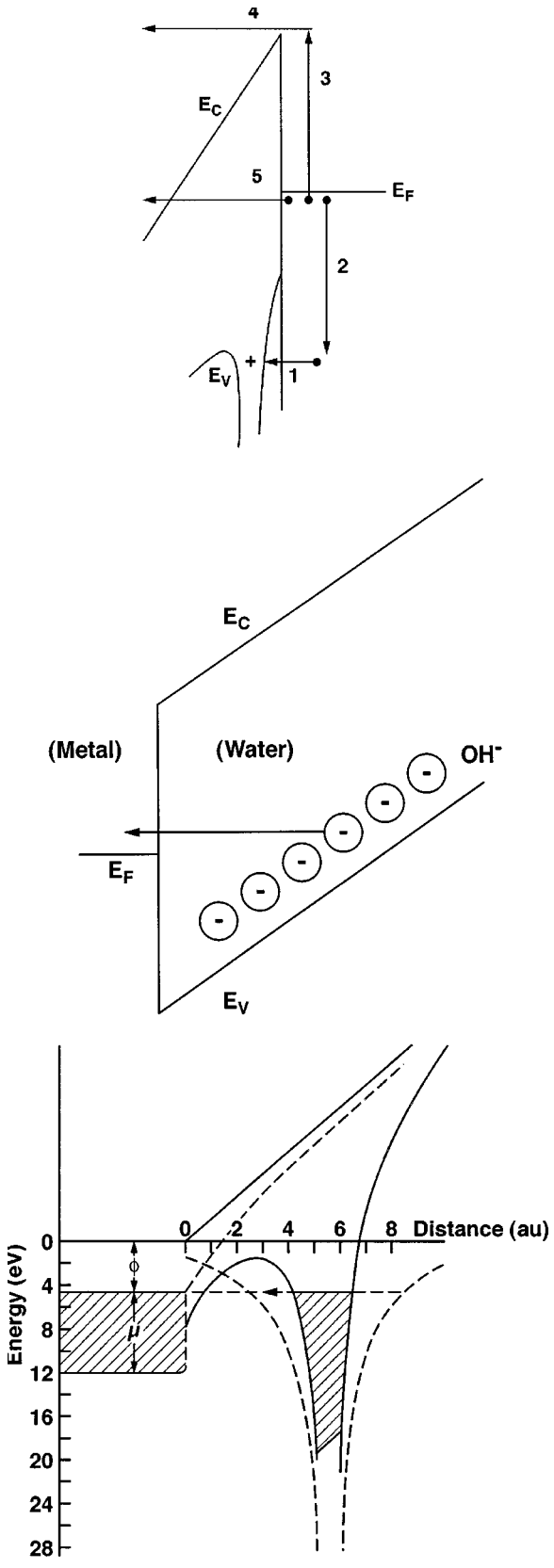

FIG. 8. Schematic of charge-transfer processes in liquid water. (a) Various electron injection processes at cathode, (b) electronic tunneling from ions at the anode, and (c) field ionization process from a neutral molecule from Ref. 49.

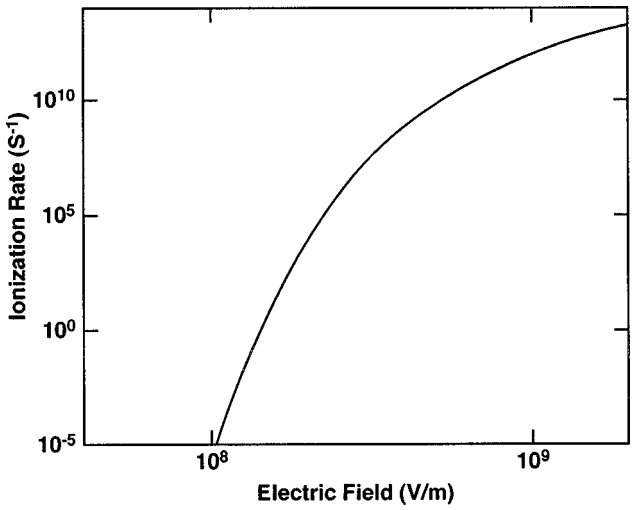

FIG. 9. Field-dependent Zener tunneling rate.

ner through a chain of neighboring molecules, provided that sufficiently high fields are accessible.

Since the precise values of effective mass, ionization energy, and molecular separation are not known, the following generic form was taken to represent the field-dependent ionization rate R_I:

$$R_I = [(qEa)/h]\exp[-K_1/E], \tag{12}$$

where K_1 is an adjustable parameter. A value of 4.27×10^9 V/m was seen to work in providing a quantitative agreement with the experimental data, as discussed in the next section. This corresponds to an effective ionization barrier of 2.3 eV. The resulting field-dependent ionization rate for this K_1 value is shown in Fig. 9. For electric fields beyond 5×10^8 V/m, a fairly high ionization rate is predicted. As will be shown in the next section, this contributes to a localized breakdown, and the high-field ionization cascades down to successive segments. It may be pointed out that field ionization does not require the presence of seed electrons nor the charge transfer. Hence, the breakdown event can propagate at the speed of the electric field and can be very fast due to the exponential dependence of the ionization rate on the field. Also, the process would not be limited by the carrier drift.

The electronic transition probability $p(E \text{ and } z)$ from the negative ions to the metallic anode as shown in Fig. 8(b) is position and field dependent and governed by the wave function overlap between the ionic location and the $z=0$ anode. Assuming a decaying exponential wave function and using the Wigner-Kramers-Brillouin (WKB) approximation[52] for tunneling from the ions to the metal through the water band gap leads to the following:

$$p(E \text{ and } z) = \exp[-\alpha z]\exp[q(\phi_m - 6.3 + Ez)/\{k_B T\}, \tag{13a}$$

for $\{z[E-\alpha k_B T/q]\} < 6.3 - \phi_m$,

$$p(E \text{ and } z) = 1.0., \tag{13b}$$

for $\{z[E-\alpha k_B T/q]\} \geqslant 6.3 - \phi_m$,

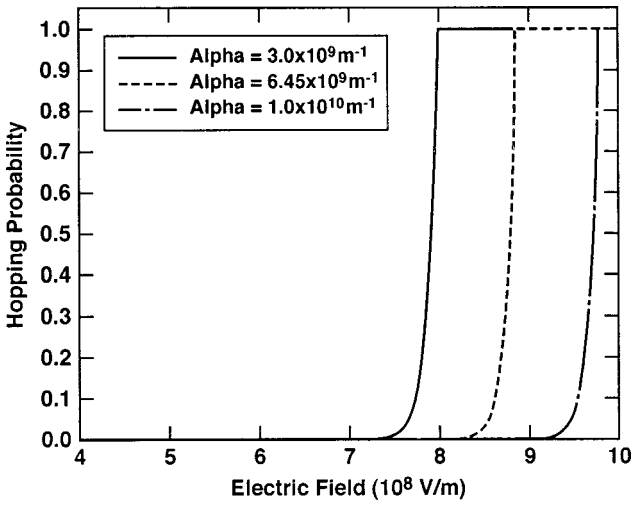

FIG. 10. Electron hopping conduction probability at the anode as a function of electric field for various a values.

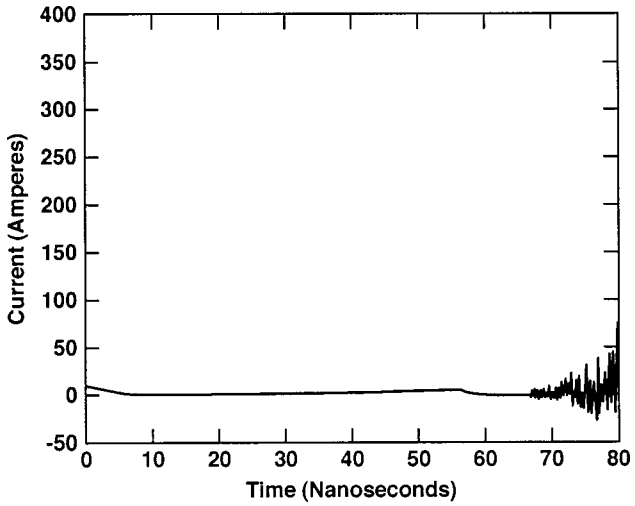

FIG. 12. Time-dependent circuit current from the simulations in response to a 40 kV, 200 ns pulse.

$$p(E \text{ and } z) = 0.0, \tag{13c}$$

for $6.3 < \phi_m$, where ϕ_m is the metal work function in electron volt and α is a characteristic parameter that describes the wave function decay. Here, the wave function (centered at the ion) was taken to be $\sim\exp[-\alpha|z|]$, with $\alpha \sim 6.45 \times 10^9\ \mathrm{m}^{-1}$. Such decaying exponential descriptions of the wave function are commonly used in the treatment of hopping conduction in ions. Figure 10 shows the plots of this anode-side probability as a function of electric field for three different α values. It is evident that (a) the tunneling probability increases with the electric field as expected, (b) the probability is higher for a metal with a larger work function, and (c) finally, a distinct field-controlled switching characteristic is evident in Fig. 11. Thus, beyond a critical anode field, a sharp transition toward a large device conduction can be expected. The work-function dependence is important, and implies that large work-function metals will facilitate a large anode current, leading to smaller hold-off voltages.

Finally, the cathode probability, p_C, for electron emission into the conduction band (process "a" of Fig. 8) can be expressed in the WKB approximation obtained as follows:

$$p_C = \exp[-\{4(2mq)^{0.5}/(3E\hbar)\}\{\phi_m - 0.1 - (qE/\{4\pi\varepsilon\})^{0.5}\}], \tag{14}$$

where E is the electric field at the cathode, $\hbar$ is the reduced Planck's constant, and ε is the permittivity. As discussed recently,[42] the permittivity can be field dependent. This aspect was taken into consideration by using a variable $\varepsilon(E)$ value. Due to the relatively large energy barrier between the metal Fermi level and the conduction band of water, this p_C value is relatively low. The dominant conduction mechanism at the cathode would be of electron flow from the metal to the positive-ion states.

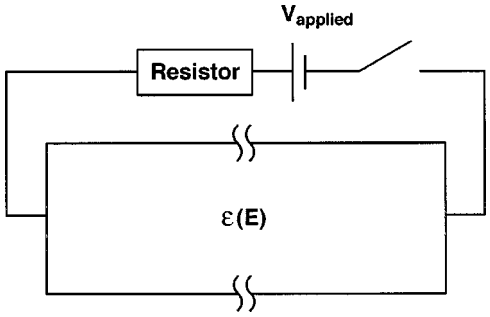

FIG. 11. Schematic of the quasi-two-dimensional continuum model used for water breakdown simulations.

IV. TIME-DEPENDENT ANALYSIS

A time-dependent simulation model was developed and implemented, as shown in Fig. 11. A 50 Ω external resistor, R, along with a supply voltage V_{app}, was placed in series with the simulation volume representing the water-filled switch device. The entire device simulation region was divided into a central region consisting of "N" boxes of equal size and characterized by ion transport on the basis of drift-diffusion (DD) theory. The DD approach was also used to update both the negative and position ion densities within each box taking account of inflows and outflows, bulk recombination and generation, charge creation due to field ionization [Eq. (11)], negative-ion generation at the cathode, positive-ion decay at the anode [based on Eqs. (13a)–(13c)], and positive-ion annihilation at the cathode via electron transfer. The existence of free electrons was neglected. Current continuity was used to update the internal electric field $E(x \text{ and } t)$ and the potential at grid points within the center of each box through the relation $J_{\mathrm{cct}}(t) = [V_{\mathrm{app}}(t) - V_{\mathrm{dev}}(t)]/R = d[\varepsilon(E)E(x \text{ and } t)]/dt + \sigma E(x \text{ and } t)$, where V_{dev} is the device voltage and $\varepsilon(E)$ is the field-dependent permittivity. Based on a detailed atomic-level analysis of the electrical response of water dipoles at the metal-liquid interface,[42] an effective field-dependent permittivity was used. This effectively leads to electric-field enhancements arising from a positive feedback mechanism, since permittivity decreases with increasing electric field. The cross sections were assumed to be rectangular, with the dimension increasing linearly from 0.85 mm at the wire to a larger 22 mm value at the plane electrode in keeping with experimental data.[9] The distance between the wire and plane electrodes was taken to be 200 μm.

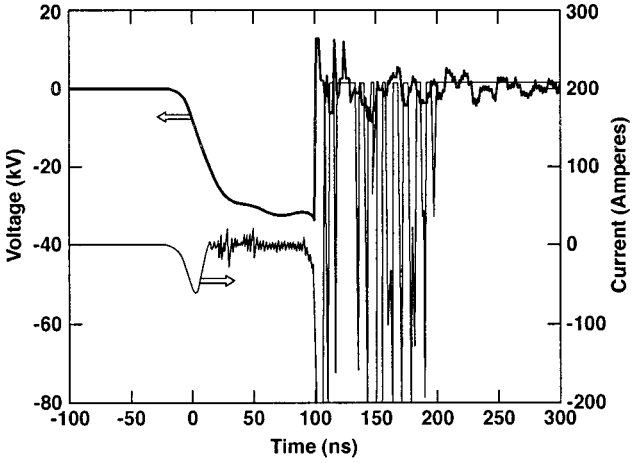

FIG. 13. Experimental data for the time-dependent circuit current for a 200 ns pulse.

The time-dependent simulation results for the previous geometry and a 200 ns, 40 kV electrical pulse were obtained by incorporating all of the charge transport and field-dependent processes. Figure 12 shows the time-dependent current for an ionization energy of 2.3 eV. The initial, sharp subnanosecond drop from a high value represents a strong displacement current. It is particularly large here because the effective inductive and/or capacitive elements were not included in the external circuit. The current is seen to quickly decay to insignificant levels until about 70 ns. Current growth and oscillations then become dominant, and breakdown is predicted. The time frame and the large characteristic current swing obtained are in good agreement with the actual experimental data shown in Fig. 13. The breakdown is predicted to be initiated at the anode and to progressively move toward the cathode. The snapshots of the longitudinal electric field along the direct anode-cathode axis at different times are shown in Fig. 14. A collapse of the electric field near the anode is predicted, with a progression toward the cathode. This is due to the buildup of a large density of negative ions at the anode side from the field ionization,

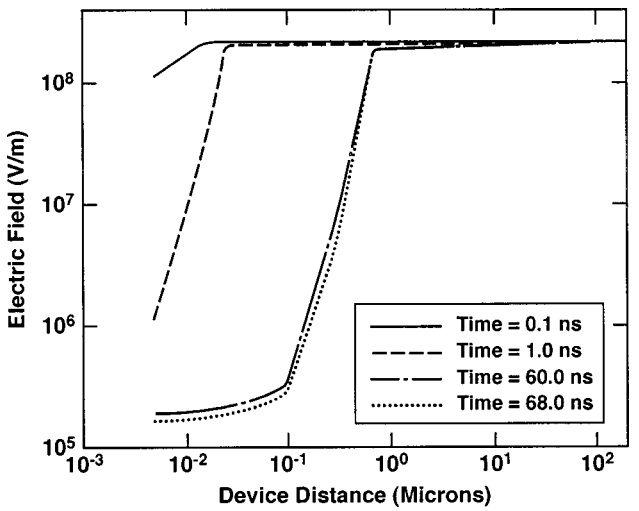

FIG. 14. Calculated distribution of the electric along the longitudinal direction at four time instants. The collapse of the field starting from the $z=0$ anode side is evident.

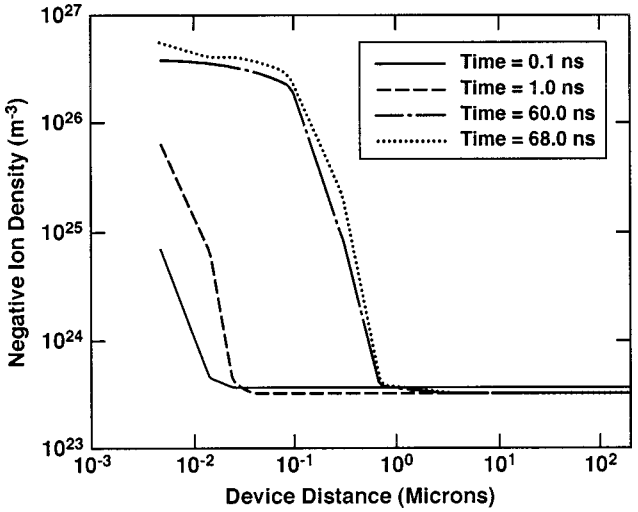

FIG. 15. Calculated distribution of the negative-ion density along the longitudinal direction at four time instants. The density is predicted to buildup with time starting at the anode.

which reduces the electric field and resistivity. Figure 15 shows the snapshots of the negative charge density at 0.1, 1.0, 60, and 68 ns from the initiation of the external pulse. Even though the equilibrium OH^- levels are roughly in the order of 3.6×10^{21} m^{-3}, values as high as 5×10^{26} m^{-3} are predicted near the anode. At times near 70 ns, this density progressively increases with the onset of the breakdown. The corresponding positive-ion densities, shown in Fig. 16, decrease with time. This is primarily due to recombination, as ionic drift velocities are generally too small to allow for the rapid carrier flush out. Quite conceivably, such recombination is likely to give rise to radiative processes, as have been observed in the experiments.

V. SUMMARY AND CONCLUSIONS

In conclusion, we have analyzed the electric breakdown process in a homogeneous liquid water for short electrical pulses in the nanosecond range. Unlike most previous break-

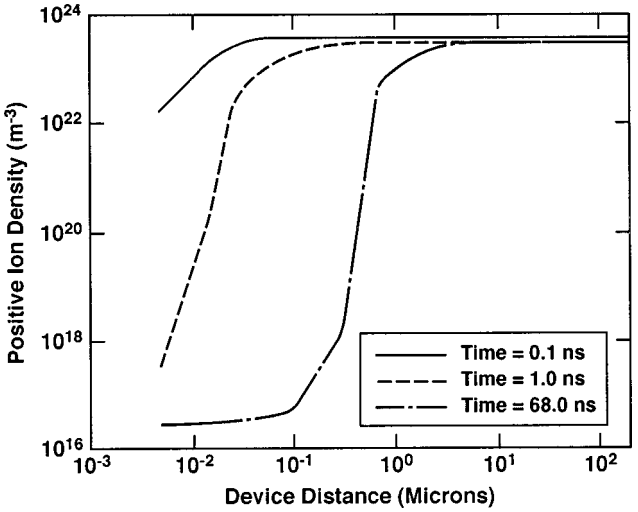

FIG. 16. Calculated distribution of the positive-ion density at three time instants. The density continually decays due to the ion recombination at the anode end.

down studies involving pulses in the microsecond range or higher, internal heating cannot be a factor in the present situation. Consequently, the liquid vaporization-related density reductions become irrelevant to the breakdown physics. In this contribution, we have attempted to probe the breakdown process based on the nonlinear, field-dependent mechanisms.

It has been shown here on the basis of Monte Carlo simulations that breakdown would not be the result of electron-impact ionization from the cathode injection. The results showed that strong elastic scattering, coupled with the highly isotropic angular deflections, prevent electrons from picking up the requisite energy. Consequently, the energy distributions were predicted to remain far below the threshold for impact ionization, despite the high external electric fields. It was also shown that only under low-density situations (as might exist due to bubble formation or partial vaporization), or upon external photoexcitation, might the electron-impact ionization process be operative. The results of the Monte Carlo analyses are also keeping with the observed polarity dependence. The electron-initiated processes would have implied a cathode initiation of the breakdown process. However, experimental data clearly indicates that breakdown is initiated at the anode and proceeds via streamers propagating toward the cathode.

A drift-diffusion model was then used in this study to probe the time-dependent dynamics of breakdown. Field ionization, as well as charge transfer at the two electrodes, and bulk recombination were all accounted for in the model. Our results indicate that field ionization (i.e., the Zener process) could only be responsible for the dramatic nonlinear increases in the current and local ion density, provided the ionization energies as low as 2.3 eV were to exist. Since this phenomena is field dependent, it is predicted to almost always start from the regions of highest electric fields, i.e., the wire electrode for the wire-plane geometries, regardless of the polarity. This is in agreement with the experimental observations. However, the relatively low-field ionization energies of $\sim$2.3 eV necessary for this scenario are somewhat unrealistic, and probably precludes this possibility.

Thus, our modeling results indicate that neither the field ionization in a homogeneous liquid water nor the electron-initiated impact ionization is likely to be the processes responsible for the experimental observations. Instead, other mechanisms not considered here would effectively be operative. Firstly, the presence of high electric fields at the contacts (especially the wire electrode) might promote the formation of nanocracks within the water as suggested recently.[53] Physically, this might arise from a net momentum transfer from either the electron swarm injected at the cathode or due to moving ions, as the charges accelerate in the high-field region. The nanocracks (or local reductions in the water density) could facilitate subsequent charges passing through the nanocrack to acquire greater energies. In time, such cracks might spread and also allow for some impact ionization. However, our preliminary analysis based on the GROMACS simulation tool,[54] which uses an atomistic approach, indicates that there would be no significant crack formation. This aspect will be reported in detail elsewhere. Next, it must be mentioned that the possibility of electron-facilitated (inelastic) field ionization was ignored here. This might be likely in the regions of large quasi-free electron populations and high electric fields. The inelastic energy loss from the quasi-free electrons could assist the field-ionization process. However, this is not likely to be very important, given the predicted lack of free and energetic electrons.[32] Experimental evidence is in support of the rapid solvation of free electrons.

The field dependent, Grotthuss-type mobility enhancements due to the proton transfers were also not considered here. However, based on the experimental data, such mobility enhancements are less than an order of magnitude.[55] So while this mechanism would certainly contribute additively to increases in the current, a breakdown or runaway phenomena would not result. Finally and more importantly, this analysis has been based on an energy-band picture, which is strictly valid for periodic, homogeneous lattices, or in the presence of long-range order. In water, however, there is no long-range order, and the constant motion of the molecular dipoles produces local fluctuations in the potential. Under such circumstances, dynamic shifts in the electronic states can be expected, leading to a field-assisted electron transfer (i.e., tunneling) between neighboring molecular sites.[56] The molecular fluctuations would provide a mechanism for bringing an occupied energy state of molecule "A" in line with an unoccupied energy state of a nearby molecule B, at least for a finite time, as the energy of individual molecules: shifted in response to structural changes. So effectively, there could be an effective field ionization based on the electron transfer during limited periods of time. However, the fluctuations in the ionization energy would be perturbative.[57] Hence, large deviations from the experimental reports of $\sim$5.2 eV ionization energies for water, based on many-body effect,[51] are not expected. Certainly, values as low as 2.3 eV as required here, would not apply for long periods of time.

The central conclusion from this quantitative analysis is that the ionization process (whether electron impact or Zener tunneling) in homogeneous, liquid water cannot be responsible for the experimental effects. A random distribution of pre-existing microbubbles within the liquid would adequately explain the observed breakdown fields and time delays. Physically, the situation would be similar to that occurring in the ceramics and nanogranular dielectrics. The strong electric fields capable of field ionization at the liquid-bubble interface would initiate the charge generation. The subsequent impact ionization within the bubble gas would create a large plasma formation and conductivity enhancements. The polarity effects would arise from the finite lifetime of free electrons in liquids. The details of the microbubble processes and quantitative results for the breakdown phenomena will be discussed elsewhere.

ACKNOWLEDGMENTS

This work was sponsored by an AFOSR-MURI with Grant No. F49620-01-1-0354 on Compact Portable-Pulsed Power. One of the authors (R.P.J.) appreciates the useful discussions with J. Lehr (Sandia National Laboratory).

[1]H. Akiyama, IEEE Trans. Dielectr. Electr. Insul. **7**, 646 (2000).
[2]J. Gaudet *et al.*, Proc. IEEE **92**, 1144 (2004).
[3]J. Talati, T. Shah, A. Memon, M. Sidhwa, S. Adil, and A. Omair, J. Urol. (Baltimore) **146**, 1482 (1991).
[4]A. H. Olson and S. P. Sutton, J. Acoust. Soc. Am. **94**, 2226 (1993).
[5]M. Zahn, Y. Ohki, D. B. Fenneman, R. J. Gripshover, and V. Gehman, Jr., Proc. IEEE **74**, 1182 (1986).
[6]M. R. Patel, M. A. Barrufet, P. T. Eubank, and D. D. DiBitonto, J. Appl. Phys. **66**, 4104 (1989).
[7]I. Vitkovitsky, *High Power Switching* (Van Nostrand Reinhold Company, New York, 1987), pp. 116–137.
[8]R. P. Joshi, J. Qian, and K. H. Schoenbach, J. Appl. Phys. **92**, 6245 (2002).
[9]S. Xiao, J. Kolb, S. Kono, S. Katsuki, R. P. Joshi, M. Laroussi, and K. H. Schoenbach, IEEE Trans. Dielectr. Electr. Insul. **11**, 604 (2004).
[10]P. K. Watson and A. H. Sharbaugh, J. Electrochem. Soc. **107**, 516 (1960).
[11]N. J. Felici, J. Electrost. **12**, 165 (1982); IEEE Trans. Electr. Insul. **20**, 233 (1985).
[12]A. Nikuradse, *Das Flüssige Dielektrikum* (Springer, Berlin, 1934), pp. 134–152.
[13]F. Pontiga and A. Castellanos, IEEE Trans. Dielectr. Electr. Insul. **3**, 792 (1996).
[14]E. E. Kunhardt, Phys. Rev. B **44**, 4235 (1991); H. M. Jones and E. E. Kunhardt, J. Appl. Phys. **77**, 795 (1995).
[15]E. O. Forster, IEEE Trans. Electr. Insul. **25**, 45 (1990).
[16]T. J. Lewis, IEEE Trans. Electr. Insul. **20**, 123 (1985).
[17]P. Keith Watson, W. G. Chadband, and M. Sadeghzadeh-Araghi, IEEE Trans. Electr. Insul. **26**, 543 (1991).
[18]A. Beroual, C. Marteau, and R. Tobazeon, IEEE Trans. Electr. Insul. **23**, 955 (1988); T. Aka-Ngnui and A. Beroual, J. Phys. D **34**, 794 (2001).
[19]J. Qian, R. P. Joshi, K. H. Schoenbach, E. Schamiloglu, and C. Christodoulou, IEEE Trans. Plasma Sci. **30**, 1931 (2002).
[20]D. J. Wales and T. R. Walsh, J. Chem. Phys. **105**, 6957 (1996).
[21]J. K. Gregory and D. C. Clary, J. Chem. Phys. **105**, 6626 (1996).
[22]P. P. Wong and E. O. Forster, IEEE Trans. Electr. Insul. **17**, 203 (1982).
[23]I. V. Lisitsyn, H. Nomiyama, S. Katsuki and H. Akiyama, IEEE Trans. Dielectr. Electr. Insul. **6**, 351 (1999).
[24]M. Szklarczyk, in *Modern Aspects of Electrochemistry*, edited by J. O'M Bockris, B. E. Conway, and R. E. White (Plenum, New York, 1993), Vol. 25, pp. 253–296.
[25]A. Larsson, A. Sunesson, J. Garmer, and S. Kroll, IEEE Trans. Dielectr. Electr. Insul. **8**, 212 (2001).
[26]R. E. Hebner, J. Phys. D **35**, 205 (2002).
[27]E. O. Forster, IEEE Trans. Electr. Insul. **20**, 891 (1985).
[28]P. K. Watson, W. G. Chadband, and W. Y. Mak, IEEE Trans. Electr. Insul. **20**, 275 (1985).
[29]J. P. Hernandez, Rev. Mod. Phys. **63**, 675 (1991).
[30]Y. Sakai, W. F. Schmidt, and A. G. Khrapak, IEEE Trans. Dielectr. Electr. Insul. **1**, 724 (1994).
[31]J. V. Coe, Int. Rev. Phys. Chem. **20**, 33 (2001).
[32]R. Laenen, T. Roth, and A. Laubereau, Phys. Rev. Lett. **85**, 50 (2000).
[33]H. M. Jones and E. E. Kunhardt, IEEE Trans. Dielectr. Electr. Insul. **1**, 1016 (1994).
[34]R. P. Joshi, J. Qian, and K. H. Schoenbach, Proceedings of the 14th IEEE International Pulsed Power Conference, Vol. 1, pp. 293–296, June 2003, Dallas (IEEE Catalog No. 03C37472C).
[35]W. Lin, J. Electrost. **36**, 129 (1995).
[36]A. Beroual *et al.*, IEEE Electr. Insul. Mag. (USA) **14**, 7 (1998).
[37]S. Katsuki, H. Akiyama, A. Abou-Ghazala, and K. H. Schoenbach, IEEE Trans. Electr. Insul. **9**, 498 (2002).
[38]Y. A. Ghazala, A. A. Zaky, and I. Y. Megahed, J. Phys. D **11**, L131 (1978).
[39]J. C. Devins, S. J. Rzad, and R. J. Schwabe, J. Appl. Phys. **52**, 4531 (1981).
[40]O. Lesaint and M. Jung, J. Phys. D **33**, 1360 (2000); P. E. Frayssines, N. Bonifaci, A. Denat, and O. Lesaint, *ibid.* **35**, 369 (2002).
[41]J. C. Martin, Proc. IEEE **80**, 934 (1992).
[42]R. P. Joshi, J. Qian, K. H. Schoenbach, and E. Schamiloglu, J. Appl. Phys. **96**, 3617 (2004).
[43]N. Agmon, Chem. Phys. Lett. **244**, 456 (1995).
[44]S. Uehara, H. Nikjoo, and D. T. Goodhead, Phys. Med. Biol. **37**, 1841 (1992); H. Nikjoo, D. T. Goodhead, D. E. Charlton, and H. G. Paretzke, Int. J. Radiat. Biol. **60**, 739 (1991).
[45]C. Champion, Phys. Med. Biol. **48**, 2147 (2003).
[46]C. Jacoboni and P. Lugli, *The Monte Carlo Method for Semiconductor Device Simulation* (Wein Publishers, New York, 1989).
[47]C. K. Birdsall and A. B. Langdon, *Plasma Physics via Computer Simulation* (McGraw Hill, New York, 1985).
[48]W. F. Schmidt, *Liquid State Electronics of Insulating Liquids* (CRC, Boca Raton, 1977).
[49]R. Gomer, *Field Emission and Field Ionization* (Harvard University Press, Cambridge, 1961).
[50]C. Zener, Proc. R. Soc. London, Ser. A **145**, 523 (1934).
[51]C. J. Rothfuss, V. K. Medvedev, and E. M. Stuve, Surf. Sci. **501**, 169 (2002); J. Electroanal. Chem. **554–555**, 133 (2003).
[52]E. Merzbacher, *Quantum Mechanics* (John Wiley, New York, 1970).
[53]T. J. Lewis, IEEE Trans. Dielectr. Electr. Insul. **10**, 949 (2003).
[54]H. J. C.Berendsen, D. van der Spoel, and R. van Drumen, Comp. Phys. Comm. **91**, 43 (1995).
[55]A. A. Kornyshev, A. M. Kuznetsov, E. Spohr, and J. Ulstrup, J. Phys. Chem. B **107**, 3351 (2003).
[56]A. M. Kuznetsov, *Charge Transfer in Physics, Chemistry, and Biology* (Gordon and Breach, Amsterdam, 1995).
[57]T. R. Mattsson (private communication).